COMPLETE PROCESSING FOR INTRAVASCULAR ULTRASOUND ELASTOGRAPHY

J. Fromageau[1,*]**, E. Brusseau**[1]**, C de Korte**[2,3,4]**, T. van der Steen**[2,3]**, D. Vray**[1]**, P. Delachartre**[1]
[1] CREATIS, CNRS Research Unit (UMR 5515), affiliated with INSERM, Lyon, France
[2]Biomedical Engineering, Thorax Center, Erasmus Medical Center, Rotterdam, the Netherlands
[3]Interuniversity Cardiology Institute of the Netherlands (ICIN)
[4] Clinical Physics Laboratory, University of Childrens Hospital, Nijmegen, The Netherlands.
*****Email: fromageau@creatis.insa-lyon.fr**

Abstract

In this paper a complete processing for intravascular elastography is presented. The technique consists in three main steps: a fully automatic blood wall interface segmentation, a strain computation and a reconstruction of a mechanical parameter. A first assessment of the developed method was performed with simulated data and a fresh excised human carotid artery. Resulting elastograms show a good agreement with medium mechanical parameters, and demonstrate the ability of the technique to produce images relative to the elasticity.

Introduction

Intravascular elastography aims at mapping the elasticity of the arterial wall during the cardiac cycle [1], [2]. This technique might provide useful information to select the most appropriate therapeutic procedure and/or to predict the disease evolution. Strain estimation methods used in intravascular elastography are those that were developed in the extracorporal investigations. But since the transducer is positioned in the lumen and not in direct contact with the tissue, an increase of pressure moves away the arterial wall from the transducer, making necessary a registration of the beginning of the wall signals acquired at different pressure levels. This preprocessing, that has to be observer independent, requires the use of a fully automatic segmentation of the blood-wall interface.

The main objective of this study is to provide a complete improved elastographic processing to investigate vessel elastic properties. The method consists of 3 main steps: the initial step is the blood-wall interface segmentation to register signals acquired before and after deformation. Then displacement and strain distributions are estimated independently. The final step is the parametric reconstruction of elasticity. Validity of the method was tested on simulated and experimental data. Resulting elastograms show a good agreement with medium mechanical parameters, and demonstrate the ability of the method to produce images relative to the elasticity.

Blood-wall interface segmentation

The approach adopted in this study is mainly a statistical one. It exploits the statistical difference between blood (denoted R_1) and tissue (denoted R_2) brightness to deform an active contour. But the main interest of the presented technique is that it requires neither parameter tuning, nor a manual pre-selection of a region of interest tight around the searched boundary. This has been achieved by an initial contour that is not set like in classical snake-based algorithms but computed, and thus adapted to each image.

Theoretical background

Ultrasound speckle is an inherent characteristic of ultrasound images. It has a random nature as formed by scatterers whose locations and acoustical strengths are randomly distributed. Echo envelop statistics depend on the effective scatterer density. Several studies have shown that ultrasound echo envelop can be well approximated by Rayleigh distributions. With this model, the probability that a pixel i, has a brightness A_i is given by :

$$P(A_i) = \frac{A_i}{\alpha^2} \exp(-\frac{A_i^2}{2\alpha^2}) \qquad (1)$$

with α the distribution parameter.

By considering the Rayleigh model, the segmentation problem becomes searching the lumen border as a continuous smooth closed curve that separates optimally two regions identified as two Rayleigh distributions, one modeling the blood brightness and characterized by the parameter α_1, the other corresponding to the tissue and characterized by the parameter α_2. A well adapted statistical procedure to determine the contour position, from an initial *a priori* contour *C* with prior probability *P(C)*, is the Bayesian estimation. The Bayesian estimator that is often used in practice is the maximum *a posteriori* (*MAP*) approach. The *a posteriori* probability $P(C|I)$ computes for a given contour position its probability to occur. The *MAP* approach thus searched the contour that has the highest probability to occur, as the argument that maximizes $P(C|I)$ (Eqn.2):

$$\widetilde{C} = \arg\max_C[P(C|I)] = \arg\max_C[\frac{P(I|C)P(C)}{P(I)}] \qquad (2)$$

with $P(C|I)$ the data model, *P(C)* the contour model, and *P(I)* the *a priori* data probability, a normalization

constant which only depends on the noise. *P(I)* is thus a constant that can be removed from the maximization problem. Finally for the sake of simplification, the logarithm of the expression is preferred, leading to:

$$\widetilde{C} = \arg\max_C [\ln[P(I|C)] + \ln[P(C)]] \qquad (3)$$

Blood and tissue brightness are modeled by Rayleigh distributions. The analytical expression of the data model is thus given by:

$$P(I|C) = \prod_{i \in R_1} P(A_i|C) \prod_{j \in R_2} P(A_j|C)$$

$$P(I|C) = \prod_{i \in R_1} \frac{A_i}{\alpha_1^2(C)} e^{\left(-\frac{A_i^2}{2\alpha_1^2(C)}\right)} \prod_{j \in R_2} \frac{A_j}{\alpha_2^2(C)} e^{\left(-\frac{A_j^2}{2\alpha_2^2(C)}\right)}$$

$$(4)$$

with α_1 and α_2 parameters that need to be estimated. Their values can be easily derived with the maximum likelihood estimation technique [3], leading to:

$$\alpha_1 = \sqrt{\frac{1}{2n_1(C)} \sum_{i \in R_1} A_i^2} \quad \alpha_2 = \sqrt{\frac{1}{2n_2(C)} \sum_{j \in R_2} A_j^2}$$

$$(5)$$

with $n_1(C)$ and $n_2(C)$ the number of samples in region R_1 and R_2 respectively, given C. By injecting (5) and (4) in (3) and removing terms whose sum leads to a constant, the final criteria becomes:

$$\widetilde{C} = \arg\max_C [-n_1(C)\ln(\alpha_1^2(C)) - n_2(C)\ln(\alpha_2^2(C)) + \ln(P(C))]$$

$$(6)$$

The MAP estimator performs well when two regions with homogeneous brightness have to be separated. However, this situation is hardly met with intravascular ultrasound images, simply because the texture of the arterial wall may be highly heterogeneous, all the more that the tissue is affected by atherosclerosis. This means that in many cases, the tissue brightness can not more be modeled by only one Rayleigh distributions but, is represented by several juxtaposed Rayleigh distributions. The consequence of this observation is that the *MAP* may be at a position that does not correspond to the luminal border. However the shape of the *a posteriori* probability gives complementary information since local maxima reveal region transitions. Moreover the heterogeneity in intravascular ultrasound images mainly occurs in the arterial wall, while the blood texture appears more homogeneous. Under these considerations, the luminal border may also be searched as the first local maximum (*FLM*) of $P(C|I)$. But because blood heterogeneity might also occur, we have decided to consider both the *MAP* and the *FLM* for the initial contour computation.

Initial contour construction

All the processing is performed on the envelope polar image. The polar image is divided in the angular direction θ in N regions of equal width. To each region is attributed a point of the contour. The contour is thus defined as a polygon with N control points M_i, whose angular positions are fixed at the middle of each region denoted Rg_i. Only their axial position r_i remain to be determined (fig.1). For the initial contour computation step, all regions are first process independently. For each region $P(C|I)$ is computed at each axial position, by virtually moving from the top downwards a border supposed to be an horizontal line. From $P(C|I)$, both the *MAP* and *FLM* positions are determined. Then, the initial contour is constructed as fol-
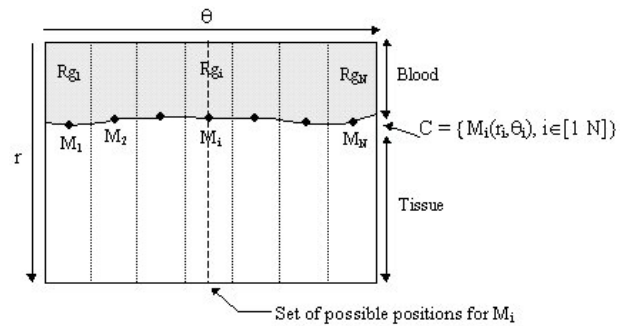

Figure 1: Problem illustration

lows : on regions where the *MAP* and the *FLM* are at the same axial position, they have a strong probability to indicate the blood-wall interface. They are termed reliable points and considered as points of the initial contour. Then, for points for which the *MAP* and *FLM* do not lead to the same axial position, the two found positions are considered as possible. By considering all the regions and the reliable points, positions retained are those that lead to the smoothest contour.

Contour evolution

Once the initial contour is determined, a region of interest of 30 pixels above and below the contour is selected. A smoothness constraint is also introduced to obtain a final smooth closed contour. It has to be noted that the smoothness constraint has been determined empirically, fixed to 0.5 and has never been changed, whatever the image to process. Thus the contour evolution consists of the iterative scheme of defining the region of interest and computing the new contour position. The algorithm stops when the contour motion becomes so small that it can be ignored.

Results

To illustrate our technique performance, automatic contours obtained for two *in-vivo* images of coronary arteries are presented in Figure 2. The first image (Fig. 2a) represents an easy situation since the catheter is positioned close to the lumen center and the blood-wall interface is characterized by a significant pixel amplitude variation. In such conditions, segmenting the luminal area presents no real difficulty. However for more complicated images, the technique still detects successfully the searched contour. One illustration is given (Fig. 2b) representing an artery with a stent restenose. On the intravascular image, the stent appears as bright spots that can negatively influence the contour detection. However results demonstrate that the active contour is not attracted by the stent and well converges towards the luminal border.
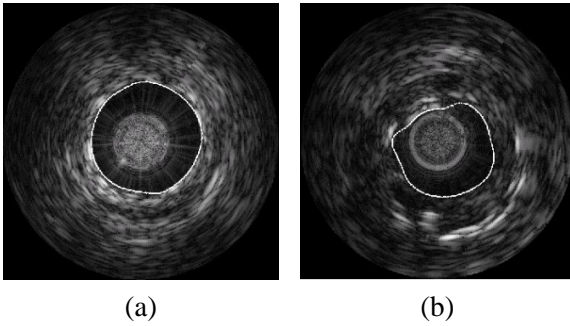

(a)   (b)

Figure 2:   Examples of automatic contour.

Strain estimation

Consider a tissue undergoing a strain ε, the signal after deformation $s(t)$ can be written as:

$$s(t) = r(t + t\varepsilon(t)) \tag{7}$$

where $r(t)$ is the reference signal. In our model the strain ε can be considered as a scaling factor ($\varepsilon(t) = cte$) or as a delay ($t\varepsilon(t) = cte$).

To estimate strains we developed an algorithm based on the maximisation of the cross-correlation of $r(t)$ and $s(t)$. The expression of the complex correlation, $R_{\widetilde{rs}}(\widehat{\varepsilon})$, according to the strain is :

$$R_{\widetilde{rs}}(\widehat{\varepsilon}) = \int_{-\infty}^{\infty} \widetilde{r}(t)\widetilde{s}^*(t - t\widehat{\varepsilon})dt \tag{8}$$

where $\sim$ indicates the analytic signal. Owing to the Hilbert transform properties the cross-correlation can be written as:

$$R_{\widetilde{rs}}(\widehat{\varepsilon}) = 2\left(R_{rs}(\widehat{\varepsilon}) - jR_{\widcheck{r}s}(\widehat{\varepsilon})\right) \tag{9}$$

where $\widecheck{}$ is the imaginary part of the analytic signal, and the Hilbert transform of the RF signaux. When the estimated strain, $\widehat{\varepsilon}$, is equal to the applied strain, ε then,

according to the equation (7), the cross-correlation becomes auto-correlation of $r(t)$, which also corresponds to the signal energy, a real and positive value. This means that the imaginary part is zero. The algorithm is actually based on the search of the root of the imaginary part of the cross-correlation using a Newton algorithm.

In the following the strain will be estimated both as a scaling factor and as a time delay. This have been performed in order to have independent measurements (see next section).

It has to be noted that the local estimation is performed by dividing the RF signals in segments and by estimating the strain for each segment. For more accurate and faster estimation, an adaptive displacement of the window of study is introduced. While moving uniformly on the reference signal, the window on the signal after deformation moves of a length which depends on the strains previously estimated.

$$\begin{aligned} t_i &= i.\Delta_T \\ t_i' &= t_i + \Delta_T \sum_{l=1}^{i-1} \widehat{\varepsilon}_l \end{aligned} \tag{10}$$

where t_i is the beginning of the ith calculation window for the reference signal, t_i' is the beginning of the ith calculation window for the deformed signal and T is the window length.

An additive processing is necessary when the scaling factor is calculated. A very accurate registration, smaller that the sample period, is then necessary to have an unbiased estimation of the strain. This additive registration is performed by calculating the delay between the two signals for the first calculation window and by compensating for.

Parametric reconstruction

Theoretical deformation of a thin cylinder

In the case of a thin cylinder its length is supposed to be large compared to the section size, and the plane strain simplification can be applied. In the case of the symmetry around the cylinder axis, the radial displacement only depends on the radius and can be expressed as :

$$u_r(r) = -\frac{A}{r} + Br \tag{11}$$

where A and B depend on the medium mechanical and geometrical properties. This relation is true for any cylinder with the described symmetry, independently of the number of layers. Radial and tangential strains are linked to the radial displacement by: (Eq.12)

$$\begin{aligned} \varepsilon_{rr}(r) &= \frac{\partial u_r}{\partial r} = \frac{A}{r^2} + B \\ \varepsilon_{\theta\theta}(r) &= \frac{u_r}{r} = -\frac{A}{r^2} + B \end{aligned} \tag{12}$$

It appears clearly that radial and tangential strains differ only by the sign of a coefficient. Then a simple summation of these two strains leads to a constant, $2B$. This sum represents the compression rate of an elementary surface and depends on the mechanical properties of the tissue. Furthermore, tangential strain can easily be deduced from displacement (Eq.12). It is also important to note that for a pure incompressible media this constant vanishes.

Thus in practical terms radial and tangential strains have been estimated as follows: the radial strain was computed with a scaling factor estimation [5], and the tangential strain was deduced from the radial displacement (Eq.12), the latter being estimated by using a time delay technique[4].

Results

The method was first assessed with simulated data corresponding to a thin cylinder exhibiting an eccentric plaque (fig.3-d). Simulated data are obtained by combining a finite element model with an acoustical field simulation software. Despite the loss of symmetry of this model, the reconstruction is applied. Both radial and tangential strain fields were estimated (Fig.3). On the radial elastogram the plaque can be located, but its shape is not obvious, whereas on the reconstructed image, even if each area does not appear homogeneous, the plaque is clearly visible. Higher strains are also visible at the plaque extremities and highlight areas where symmetry is low.
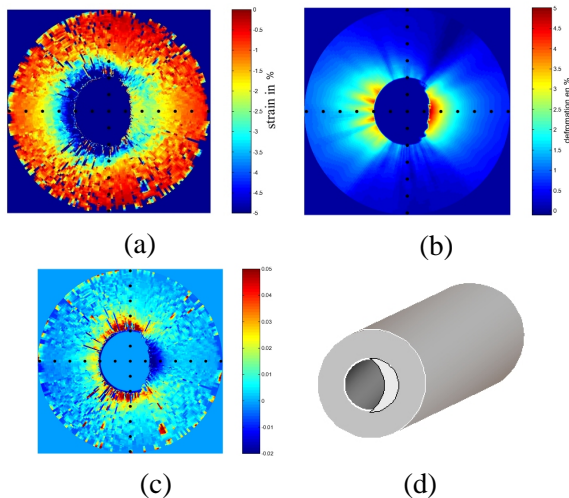

(a)   (b)

(c)   (d)

Figure 3: Elastograms for simulated phantom with an hard eccentric plaque. a) radial strain b) tangential strain c) strains summation d) elasticity distribution

The reconstruction was also tested on a fresh excised human carotid artery (fig.4). The radial elastogram permits to detect an area of low strain, revealing a hard plaque, but whose shape is not accurate. On the recon-

structed image the plaque area appears more clearly and matches with the histological section. These first images on an *in vitro* artery show encouraging results.
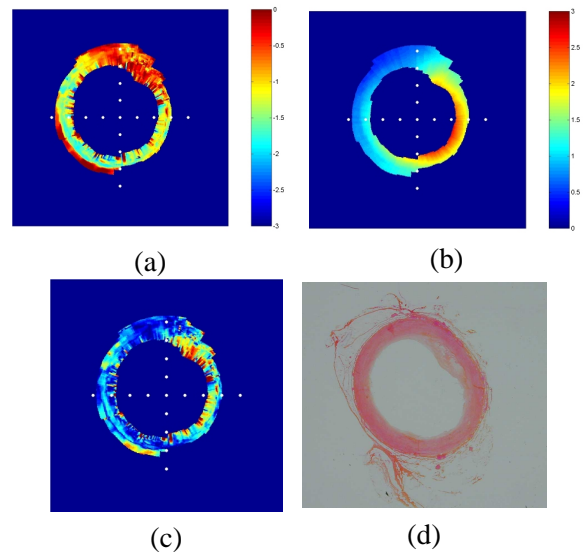

(a)   (b)

(c)   (d)

Figure 4: Elastograms for an *in vitro* carotid artery with a thin plaque. a) radial strain b) tangential strain c) strains summation d) histological section

Conclusion

In this paper a complete processing for the investigation of elasticity in intravascular elastography has been introduced. Results on simulations and an *in vitro* carotid artery have demonstrated the potentiality of our technique.

References

[1] C.L. de Korte, A.F.W van der Steen, "Intravascular ultrasound elastography: an overview," Ultrasonics, vol 40, pp. 859-865, 2002.

[2] B.M. Shapo, J.R. Crowe, A.R. Skovoroda, M.J. Eberle, N.A. Cohn and M. O'Donnell, "Displacement and Strain Imaging of Coronary Arteries with Intraluminal Ultrasound," IEEE Trans. UFFC., vol 43, no 2, pp. 234-246 ,1996.

[3] E. Brusseau, C. L de Korte, F. Mastik, J. Schaar, A. F W van der Steen, "Fully automated Contour Detection in Intracoronary Ultrasound Images - A pre-processing for Intravascular Elastography", IEEE Inter. Ultrason. Symp., Munich, Allemagne, 2002, p.1869-1872.

[4] A. Pesavento, C. Perrey, M. Krueger, H. Ermert, "A Time Efficient and Accurate Strain Estimation Concept for Ultrasonic Elastography using Iterative Phase Zero Estimation," IEEE Trans. UFFC, vol 45, no 5, pp. 1057-66, 1999.

[5] E.Brusseau, C.Perrey, P.Delachartre, M.Vogt, D.Vray, H.Ermert, "Axial Strain Imaging Using Local Estimation of the Scaling Factor from RF Ultrasound Signals," Ultrason. Imaging, vol 22, no 2, pp. 95-107, 2000.